ORIGINAL ARTICLE

The effect of Ta additions on the oxidation resistance of SPS-produced TiAl alloys

Prince Valentine Cobbinah[1] · Wallace Matizamhuka[1] · Ronald Machaka[2,3] · Mxolisi Bredon Shongwe[4] · Yoko Yamabe-Mitarai[5]

Abstract

The influence of the environment on the properties of TiAl alloys is a concern for elevated temperature applications. One element that stands out in improving the resistance of TiAl alloys against high-temperature oxidation is Nb. Nb promotes the activities of Al and favors the formation of a more protective Al_2O_3 surface oxide which subsequently stymies oxygen diffusion to the alloy. Ta is an equal replacement of Nb. Thus, this study aims to evaluate the effect of 0.8, 4, and 8 at. % Ta additions on the oxidation resistance of spark plasma sintered Ti-46.5Al (at. %) alloy. Isothermal oxidation tests were carried out for 360 and 100 h at 1123 and 1273 K respectively. Surface oxides examination include scanning electron microscopy with energy-dispersive X-ray spectroscopy and X-ray diffractometry. The results show that 4 and 8 at. % Ta additions significantly support the formation of an interconnected, non-porous Al_2O_3 layer at the metal-oxide interface. The continuous non-porous Al_2O_3 layer serves as a diffusion barrier which leads to superior oxidation resistance of the TiAl alloys.

1 Introduction

Over the years, TiAl-based alloys, have competently replaced nickel-based superalloys for specific temperature and stress ranges because of desirable properties [1, 2] such as low density (3.9–4.2 g.cm^{-3}), low diffusion coefficient, good corrosion, and oxidation behavior at elevated temperatures, good thermal conductivities and are ductile at their service temperatures while also maintaining good structural stability. However, TiAl alloys are known to exhibit an unbalance of strength and ductility at room temperature. Most researchers have attempted to balance this room temperature "ductility-strength imbalance" by way of microalloying with elements such as Cr, Mn, V, W, Mo, Si, B, C, Zr, and Hf to form ternary or quaternary alloys [3–7], but at the expense of oxidation resistance [8, 9].

Recent research efforts have focused on a class of materials intended in enhancing high-temperature strength, room temperature ductility, and particularly oxidation resistance have been predominantly based on the addition of Nb [2, 10–14]. From the numerous studies, Nb has proved effective in markedly increasing the resistance of TiAl alloys against elevated temperature oxidation. Nb promotes the formation of Al_2O_3, which is a denser, adherent, and protective scale compared with TiO_2 by increasing the activity of Al [15].

Ta, on the other hand, can equally substitute Nb. Their positions on the periodic table suggest that the chemical behaviors of both elements are alike. Additionally, Ta has a high-melting temperature, thus, presents the opportunity of increasing the service temperature of TiAl-based alloys. Research into the influence of Ta on the oxidation resistance of TiAl-based alloys are rarely reported in literature and appears to be,

✉ Prince Valentine Cobbinah
prinzcobbs@gmail.com

1 Department of Metallurgical Engineering, Vaal University of Technology, Andries Potgieter Blvd, Vanderbijlpark, Gauteng 1911, South Africa

2 Advanced Materials and Engineering, Manufacturing Cluster, Council for Scientific and Industrial Research, Pretoria, South Africa

3 School of Mining, Metallurgy and Chemical Engineering, University of Johannesburg, Johannesburg, South Africa

4 Institute for NanoEngineering Research, Department of Chemical, Metallurgical and Materials Engineering, Tshwane University of Technology, Pretoria, South Africa

5 National Institute for Materials Science, Sengen 1-2-1, Tsukuba, Ibaraki 305-0047, Japan

despite this knowledge, having contradicting findings. For instance, Shida and Anada [16] concluded in their study that Ta additions played no role in the oxidation resistance of Ti-48.6Al (at. %) alloy. Other studies, [17–19] reported that Ta additions were not significantly effective compared with Nb against oxidation, especially at higher temperatures. Conversely, Popela and co-workers [20] in a comparative study of Ti-46Al-8X at % (X = Ta or Nb) showed enhanced oxidation resistivity in the Ta-containing TiAl-based alloy. The oxidation resistivity was made apparent in the weight reductions of the alloy.

Thus, more knowledge and clarity are still required on the efficacy of Ta on the oxidation resistance of TiAl-based alloys. This study, therefore, aims to evaluate the effect of Ta additions on the oxidation resistance of spark plasma-sintered (SPS) TiAl-based alloys.

2 Material and methods

2.1 Synthesizing of targeted alloys

Table 1 shows the elemental powders supplied by LGC Industrial Analytical, South Africa.

Using the Retsch PM 400 high energy ball mill equipment with a 250 ml zirconia vial and grinding balls of 1-mm diameter, individual elemental powders were first milled. The Al and Nb powders were milled with the aid of 2 wt.% stearic acid process control agent (PCA) while Ti and Cr were ball milled with ethanol as PCA. Milling of the individual elemental powders was carried out at a speed of 350 rpm. Al powder was milled for 6 h whereas Nb, Ti, and Cr were milled for 4 h each. The ball-to-powder mass ratio (BPR) used for all the milling process was 5:1.

The targeted alloys, as summarized in Table 2, were loaded into a 500-ml plastic container, tightly sealed, and then placed in a Turbula® shaker-mixer for 4 h. After, the mixed compositions were mechanically alloyed using the Retsch PM 100 high energy ball mill employing a 500-ml tungsten carbide vial and stainless steel grinding balls of diameters 10,15, and 20 mm. For each alloy, the weighed PCA used was 6 wt.% of total powder mass charge per each tailored composition. Mechanical

Table 1 Elemental powders supplied, their purity, and particle sizes

Elemental powder	Purity (%)	Particle size (μm)
Titanium (Ti)	99	< 45
Aluminum (Al)	99.5	7–15
Chromium (Cr)	–	< 45
Niobium (Nb)	99.8	< 45
Tantalum (Ta)	–	≈2

Table 2 Compositions of targeted alloys

Alloy	Composition (at. %)
Reference	Ti-48Al-2Cr-2Nb
1	Ti-46.5Al-0.8Ta
2	Ti-46.5Al-4Ta
3	Ti-46.5Al-8Ta

alloying was done for 6 h for each composition at a speed of 350 rpm and a BPR of 10:1.

The FCT H-HP D25 hybrid spark plasma sintering equipment (FCT Systeme GmbH, Germany) was used in consolidating and sintering of the alloys. The process was carried out in a vacuum atmosphere, making use of a graphite die of inner diameter 100 mm, graphite punches and graphite foils—which were used to line the flat ends of the die [21]. With a heating rate of 473 K.min^{-1}, an applied pressure of 32 MPa and a dwell time of 10 min, sintering was done at 1423 K.

The as-sintered alloys were heat-treated for 2 h at 1673 K and 1523 K for the reference alloy and the alloys 1, 2, and 3 respectively. The heat treatment temperatures chosen were for achieving a lamellar microstructure for the reference alloy and a duplex microstructure for alloys 1, 2, and 3 [1]. The heat-treated samples were sectioned to dimensions of an average of 8 × 8 × 3 mm, ground with a 320-grit paper and cleaned with acetone. Isothermal oxidation testing at 1123 K (360 h) and 1273 K (100 h) in air were carried out in a muffle electric furnace (AS-ONE). At intervals, the samples were removed from the furnace then allowed to cool in air for 20 min and their weights measured using the SEFI AS-ONE analytical balance with an accuracy of 0.1 mg.

Metallographic examinations were done on the transverse face of the oxidized samples. Samples were ground and polished to 3 μm surface finish using the respective polycrystalline diamond suspensions. Formed oxides were examined on the surface and cross-section of the samples using the JSM-IT500 and JSM-7200F scanning electron microscope (SEM) equipped with an energy dispersive spectroscope (EDS). The MiniFlex 600 X-ray diffractometer (XRD) (Rigaku Corporation) was further used to analyze the reaction products formed on the oxidized samples. The Zeiss Stemi 305 stereomicroscope was also used to analyze the surface appearance of the oxidized samples.

3 Results

3.1 Surface appearance of oxidized samples

As shown in Fig. 1a, the reference alloy after oxidation at 1123 K is covered in a mixture of black spots and brown-

Fig. 1 The surface appearance of **a** reference alloy **c** alloy 1 and **e** alloy 2 after oxidation testing at 1123 K; **b** reference alloy **d** alloy 1 and **f** alloy 2 after oxidation testing at 1273 K
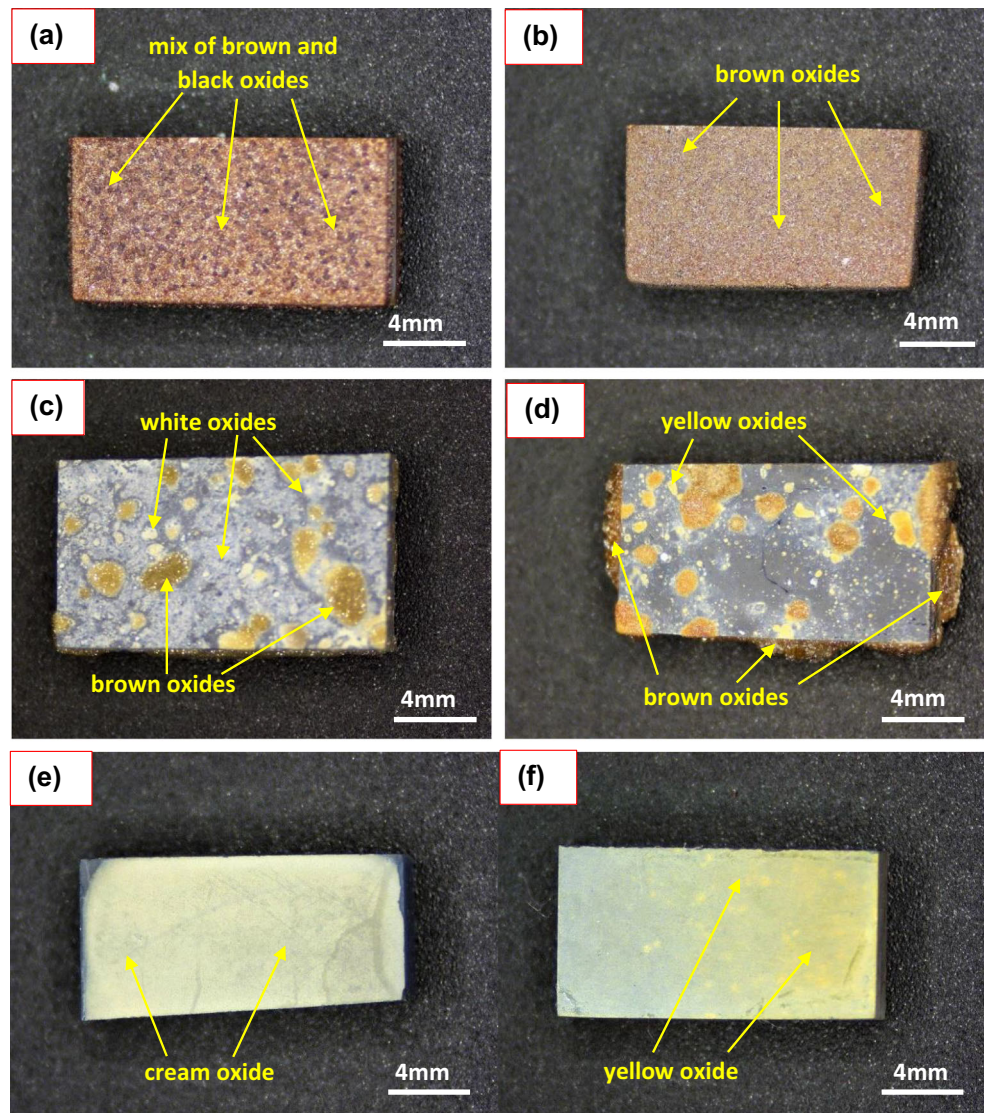
colored products with a good mix of "shiny" reflections in the brown oxides. At 1273 K, only brown-colored oxides with reflections cover the reference alloy after oxidation (Fig. 1b). Alloy 1, however, at 1123 K is covered mostly in white-colored oxides and also spots of brown-colored porous-looking oxides (Fig. 1c) with "shiny" reflections in the brown oxides. At 1273 K, no white-colored oxides are seen on alloy 1 and the quantity of brown-colored oxides increase which are mostly seen on the edges, Fig. 1d. Furthermore, spots of yellow-colored oxides are also seen on alloy 1 at 1273 K.

A uniform cream-colored film covers the surface of alloy 2 after oxidation at 1123 K as shown in Fig. 1e. At 1273 K, a yellow, relatively dense, colored layer is observed on the surface of alloy 2. Although not included in Fig. 1, alloy 3 depicts similar surface appearance as alloy 2 at both exposed temperatures and durations.

3.2 Mass change evaluation

Mass change per unit area of exposed samples versus time graphs of the alloys are illustrated in Fig. 2a and b. As noticed, all the oxidized alloys exhibit weight gains. The reference alloy and alloy 1 weight gains increase with increasing oxidation time at both isothermally held temperatures. This is consistent with some previous studies involving the 48-2-2 reference alloy [22, 23]. At 1123 K, the weight gain of the reference alloy after 360 h is about four orders (0.24 mg.mm^{-2}) more than that gained after 24 h (0.06 mg.mm^{-2}). The influence of temperature on the oxidation resistance of alloy 1 is explicit from the two graphs. Thus, at 1123 K, the relative reduction in the slope of the curve with oxidation time suggests a more protective oxide forms on the surface of alloy 1. Additionally, alloys 2 and 3 show superior oxidation resistance with minimal increase in weight at both temperatures after exposure.
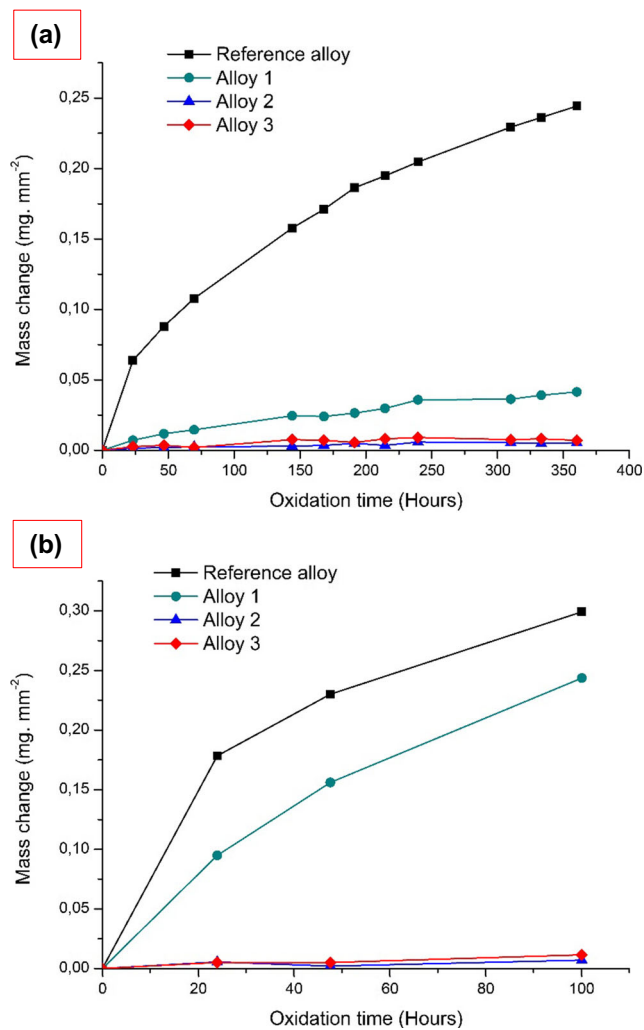
(a)

(b)

Fig. 2 Mass change graph of alloys at **a** 1123 K and **b** 1273 K oxidation testing in air

The oxidation kinetics of the alloys were calculated by the parabolic oxidation rate law according to the equation below [24]:

$$(\Delta M)^2 = K_p t$$

where ΔM is mass change per unit surface area (mg.mm^{-2}), K_p is the parabolic rate constant (mg^2.mm^{-4}.hr^{-1}), and t is the exposure time (hrs). The rate constant versus time graph of the oxidized alloys at 1123 K and 1273 K are shown in Fig. 3. The oxidation constant varies from 1.7×10^{-4} to 9.4×10^{-8} mg^2.mm^{-4}.hr^{-1} for the oxidized alloys at 1123 K.

The reference alloy exhibits a transient oxidation behavior followed by a steady-state behavior [25], whereas the ternary alloys exhibit only a steady-state behavior at 1123 K. The initial large oxidation rate of the reference alloy implies no protective oxide develops to slow the oxidation process hence making up the transient region. However, after 190 h, it can be deduced that a protective layer forms leading to the

continuous reduction of the oxidation rate constant till the end of the test. At 1273 K, the reference alloy seems to form a protective layer after the first 24 h of exposure. Furthermore, alloys 1, 2, and 3 obey a true parabolic oxidation behavior at 1123 K with a nearly constant oxidation rate constant in good agreement with parabolic growth [24]. Unlike alloy 1, similar oxidation behaviors are observed for alloys 2 and 3 at 1273 K. The constant oxidation rate indicates that the kinetics involved in the oxidation of alloy 2 and 3 is diffusion controlled.

3.3 XRD analysis of surface oxides

The predominant oxides from the XRD analyses in Fig. 4 are TiO_2 (rutile) and Al_2O_3. At 1123 K, TaO peaks emerge for the Ta-containing alloys. At a higher oxidation temperature of 1273 K, the patterns reveal the presence of AlTa, TaO, and Ta phases on alloys 1, 2, and 3 in addition to Al_2O_3 and TiO_2 phases found on the reference alloy. Moreover, at 1273 K, the TiO_2 peaks at 42°, 54°, 63°, and 70° diminish significantly in alloys 1, 2, and 3. The XRD patterns at both tested temperatures show no presence of the nitrogen effect or nitride phases such as TiN or Ti_2AlN associated with the oxidation of TiAl alloys in air [13, 26–28].

3.4 Surface oxides morphology

Figures 5 and 6 show the surface morphology of the oxides formed on the alloys oxidized at 1123 K and 1273 K. At 1123 K, the morphology of the oxide on the outermost surface of the reference alloy and alloy 1, as arrowed, is blocky and randomly oriented. This morphology is typical of TiO_2 and is consistent with reported studies [29]. The growth of TiO_2 grains leads to the formation of various voids and pores at the grain boundaries [30]. TiO_2 on alloy 1 grow as islands and connect, as noticed in Fig. 5b and Fig. 6b. On the other hand, fine and smooth surface grains of oxide with a dark contrast form underneath the TiO_2 (Fig. 5b and Fig. 6b). The "mat-looking" continuous nature of the oxide is a good indication that the oxide is Al_2O_3. Moreover, the SEM images highlight the compactness, good adherence, and protective features of the Al_2O_3 oxide compared with TiO_2. Similar morphologies of both oxides on alloy 1 are seen on alloy 2 (Fig. 5c). However, compared with alloy 1, decreased quantities of TiO_2 form at the outermost parts of the oxides on alloy 2. Also, underneath the rutile the grains of formed Al_2O_3 oxide are bigger compared with that seen on alloy 1. On alloy 3, Al_2O_3 oxide makes up the primary oxide on the surface (Fig. 5d). The grains of formed Al_2O_3 on alloy 2 and 3 are interconnected, non-porous, and exhibit agglomeration but are irregular in shape.

At 1273 K, Al_2O_3 oxide develops at the grain boundaries of the rutile as seen in the reference alloy, alloy 1

Fig. 3 Rate constant versus time
graph of oxidized alloys at **a**
1123 K and **b** 1273 K
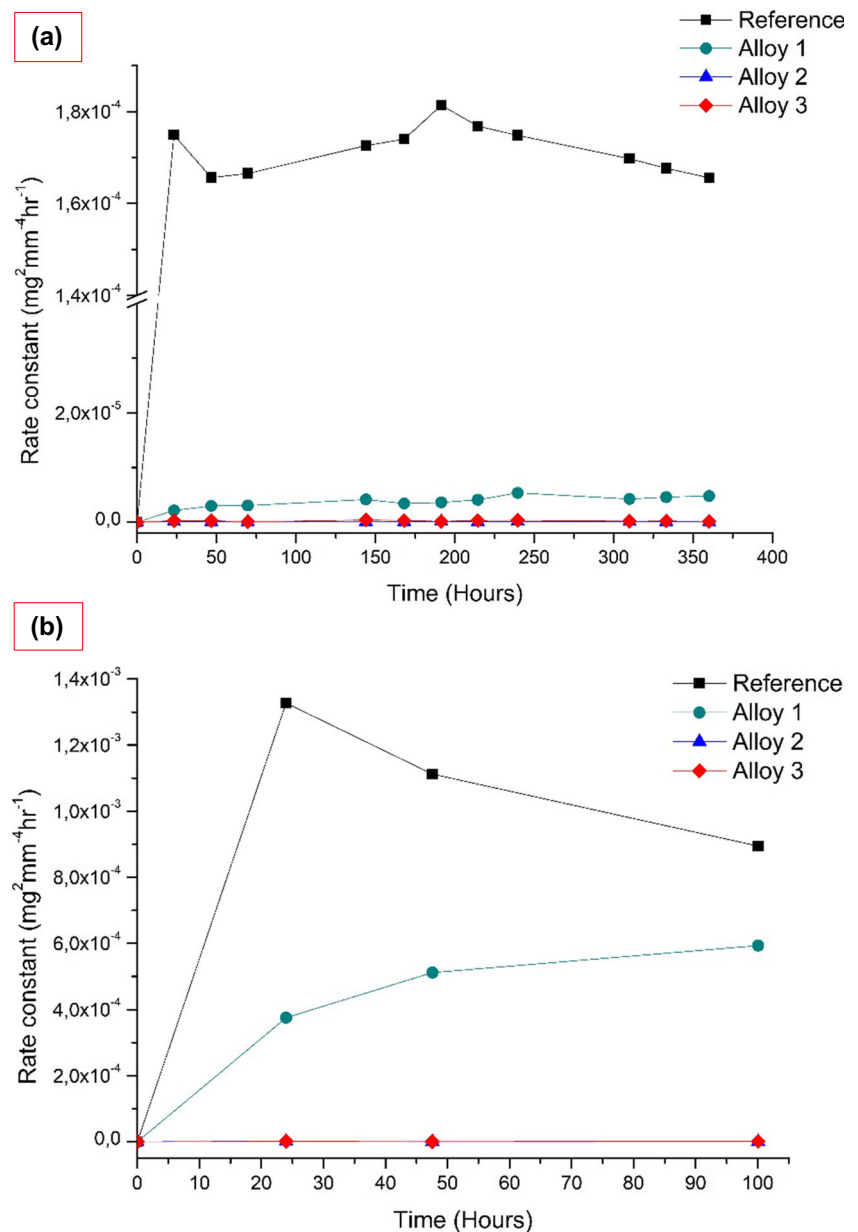
and 2 (Fig. 6a–c). The continuous growth of the Al_2O_3 oxide on alloy 2 leads to the reduction of grain sizes of TiO_2 oxide and switch in positions of the oxides. Al_2O_3 oxides become the outermost oxide film on alloy 2 and 3 (Fig. 6d) with TiO_2 forming underneath.

Similar morphologies of Al_2O_3 and TiO_2 oxides have been observed in studies by [31, 32].

3.5 Cross-section observation of oxide scale

The oxidation resistance of TiAl-based alloys is primarily characterized by the properties of the formed oxides, i.e., their morphology, stability, and density [1]. Figures 7 and 8 show the SEM secondary and backscattered electron images of the morphologies of the cross-sections of the oxides formed on the studied alloys after isothermal oxidation tests at 1123 and 1273 K respectively. The SEM-EDX line analysis in Fig. 9 further corroborates the oxides formed on the alloys as well as their relative positions.

Figure 7 a and b and Fig. 8 a and b show that a less dense TiO_2 oxide form on the outermost surface of the reference alloy and a mixture of TiO_2 and Al_2O_3 oxides at the subsurface after the different durations of exposure at 1123 K and 1273 K.

After oxidation at 1123 K, TiO_2 oxide forms at the outermost part of the oxides for alloy 1. In addition, a continuous Al_2O_3 oxide and mixed oxides of TiO_2 and

Fig. 4 XRD analysis of oxidized alloys after oxidation testing at **a** 1123 K and **b** 1273 K
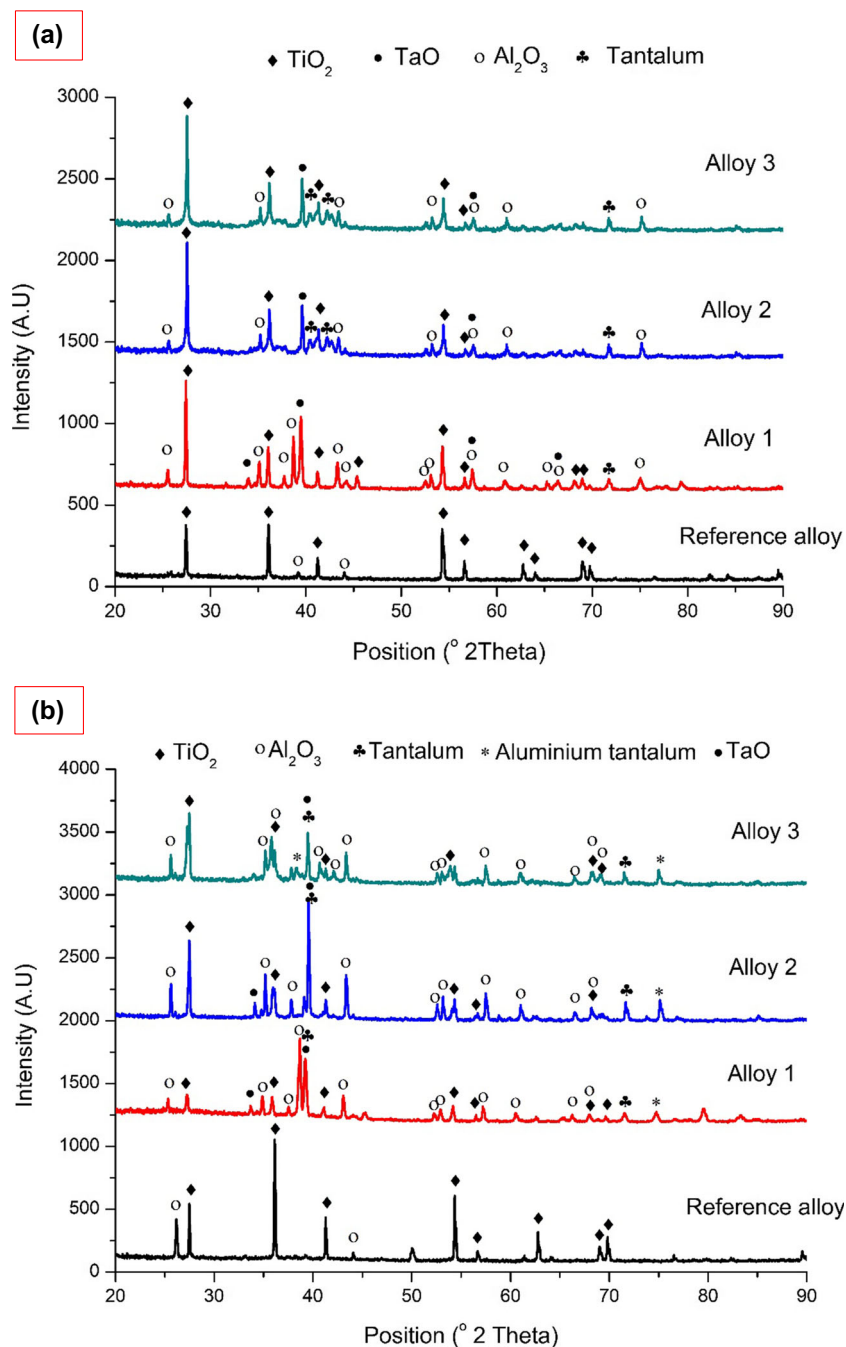
Al_2O_3 form underneath the rutile, as shown in Fig. 7c and d. Conversely, mixed oxides of Al_2O_3 and TaO develop at the outermost part of the oxides above the TiO_2 at 1273 K for alloy 1, as depicted in Fig. 8c reinforcing the influence of temperature on the oxidation resistance of alloy 1 observed from the mass change graphs.

Considering alloy 2 and alloy 3, the oxide on the surface of the alloys include a continuous compact oxide of Al_2O_3 at the outermost, as depicted in Fig. 7e–h and Fig. 8d–f.

4 Discussions

During high-temperature oxidation, the surface of the TiAl alloys adsorbs dissolved oxygen atoms. Concurrently, Ti and Al also diffuse towards the surface. In areas over-saturated with oxygen atoms, the nucleation of TiO_2 occurs [31]. Owing to the strong oxygen affinity of Ti, two possible thermodynamic chemical reactions can occur. They include [33];

$$Ti(s) + \frac{1}{2}O_2(g) \rightarrow TiO(s)$$
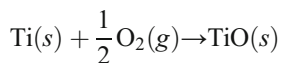
Fig. 5 Surface oxides morphology of **a** the reference alloy, **a** alloy 1, and **c** alloy 2, and **d** alloy 3 after oxidation testing at 1123 K
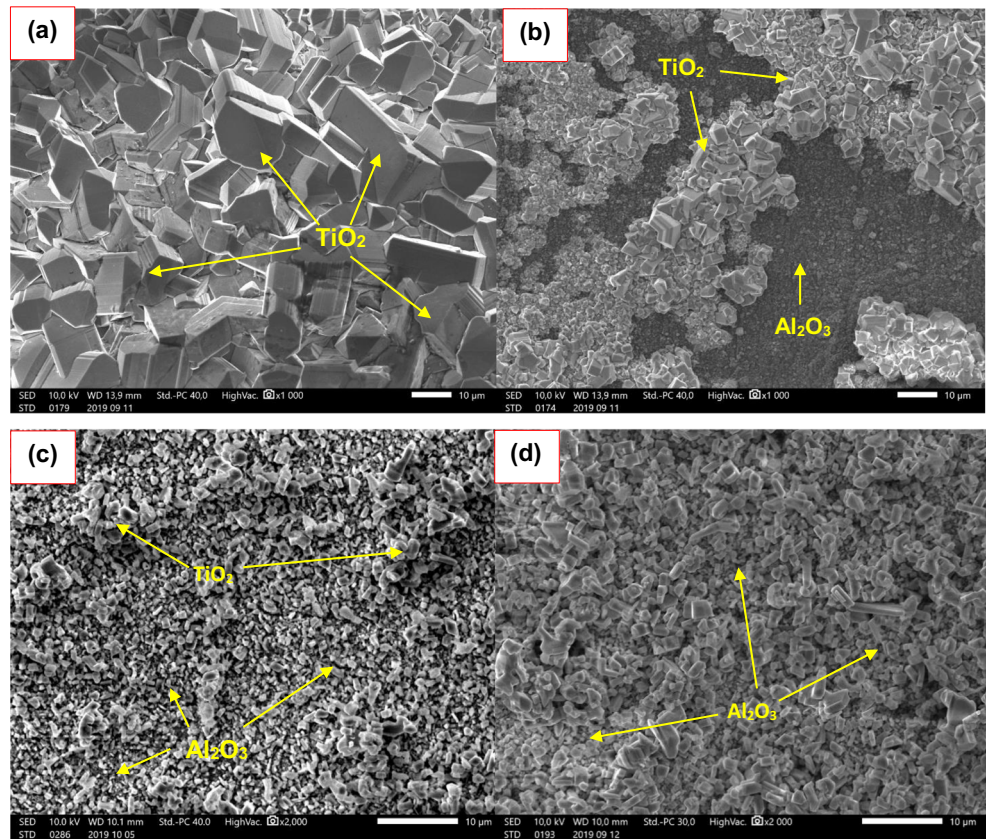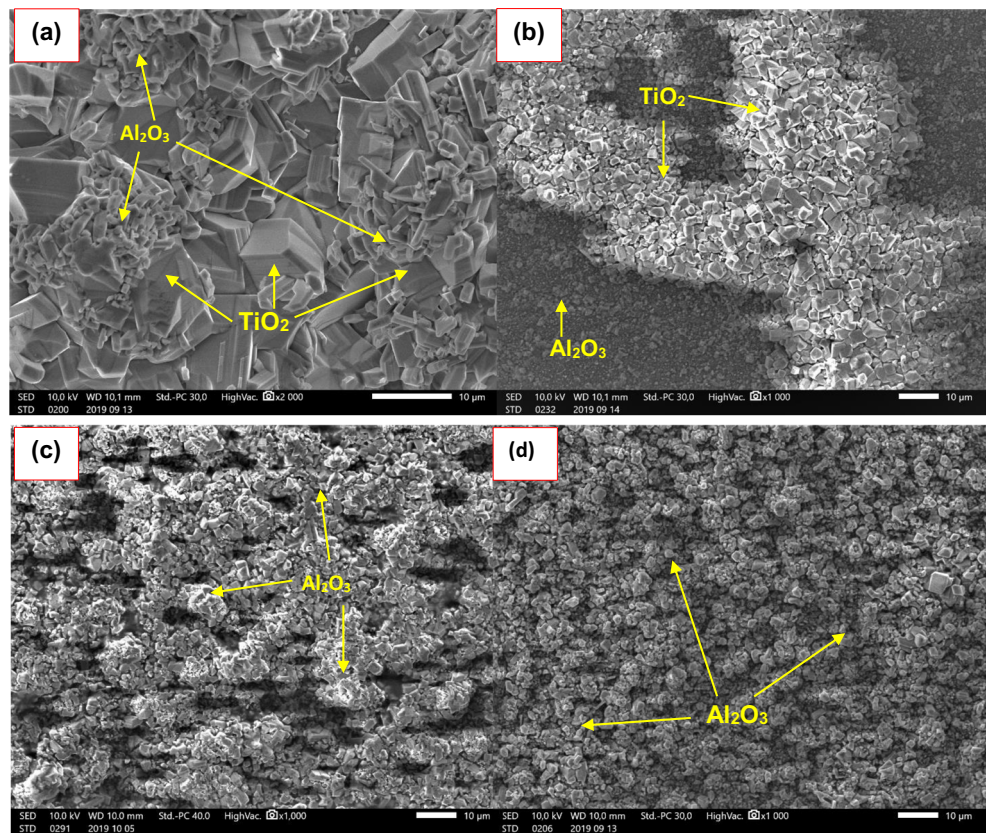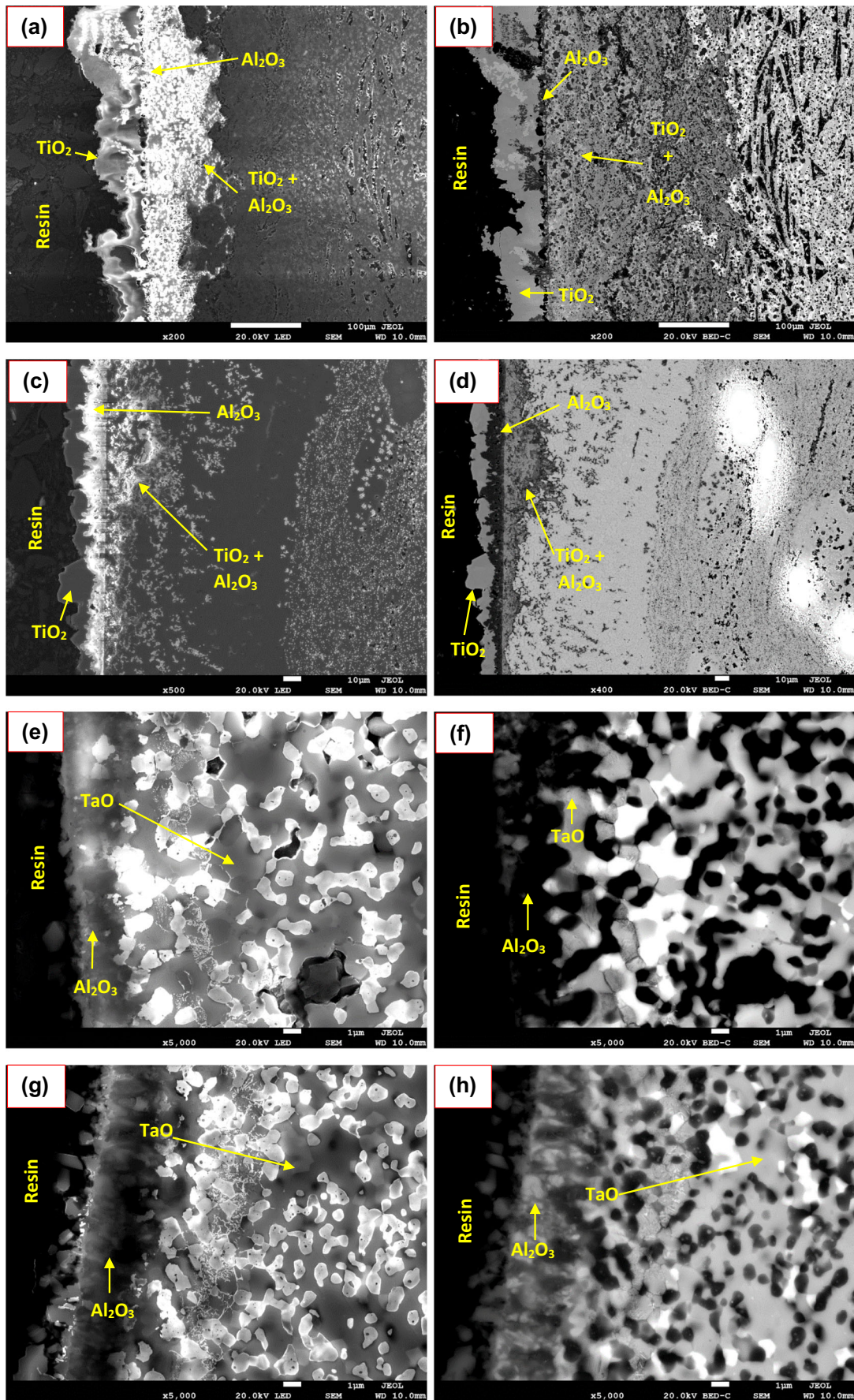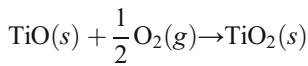

Fig. 6 Surface oxides morphology of **a** the reference alloy, **b** alloy 1, **c** alloy 2, and **d** alloy 3 after oxidation testing at 1273 K
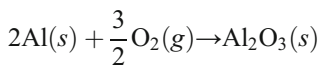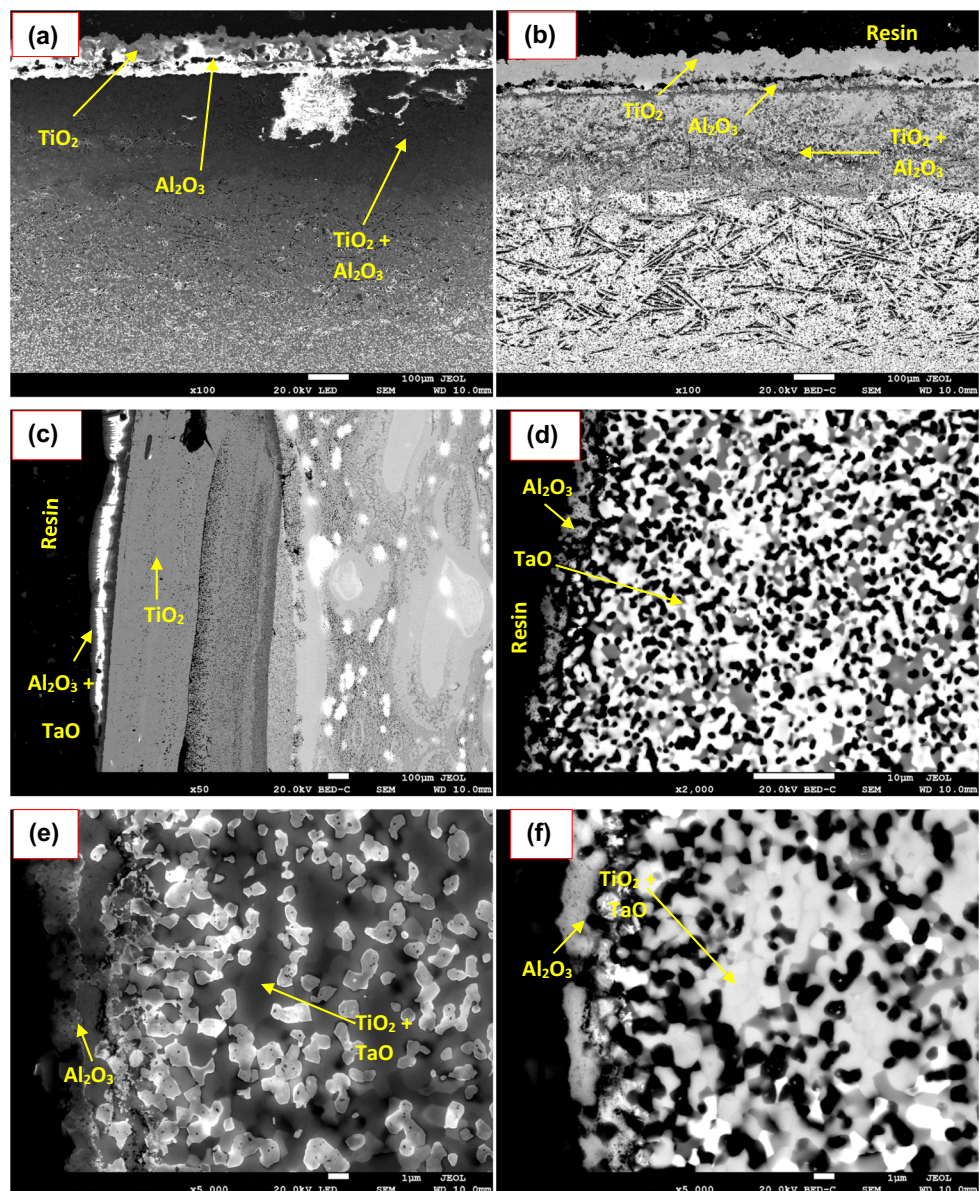
$$TiO(s) + \frac{1}{2}O_2(g) \rightarrow TiO_2(s)$$

The TiO_2 nuclei then grow laterally and form an oxide film. As a result, a local Al-rich region develops underneath the TiO_2 film favoring the further formation of Al_2O_3 according to the reaction [34];
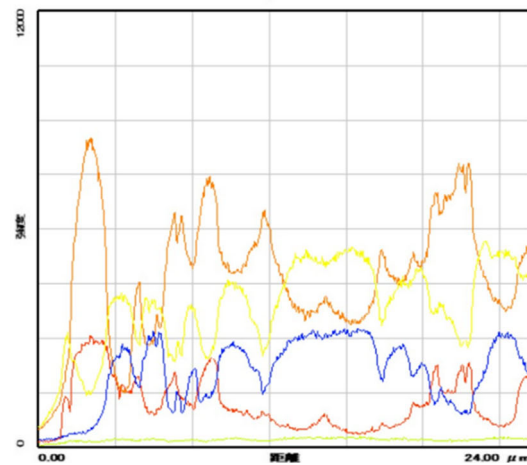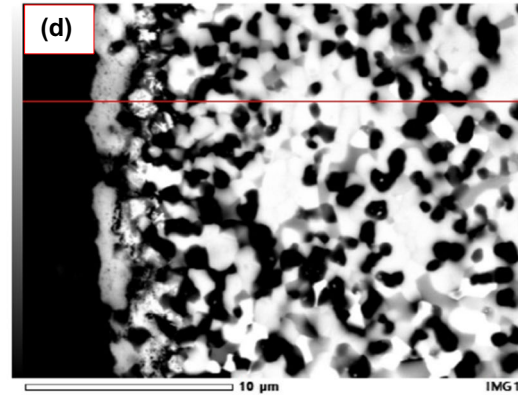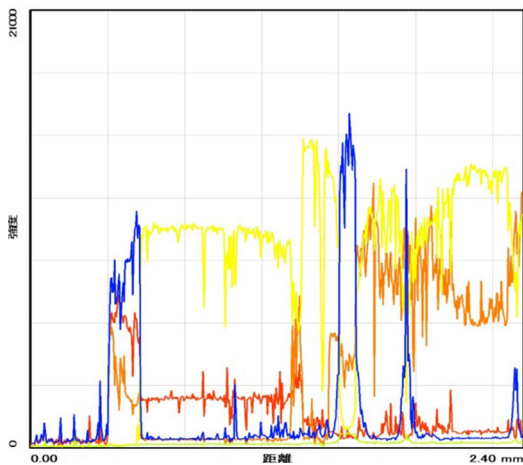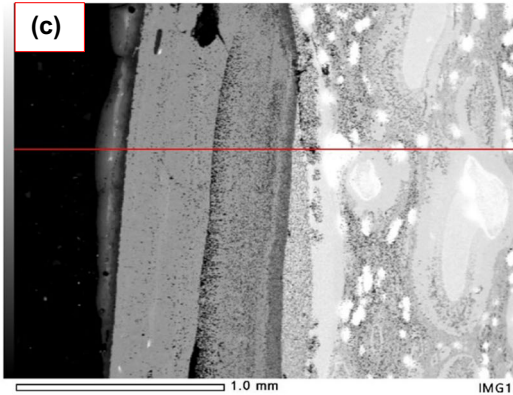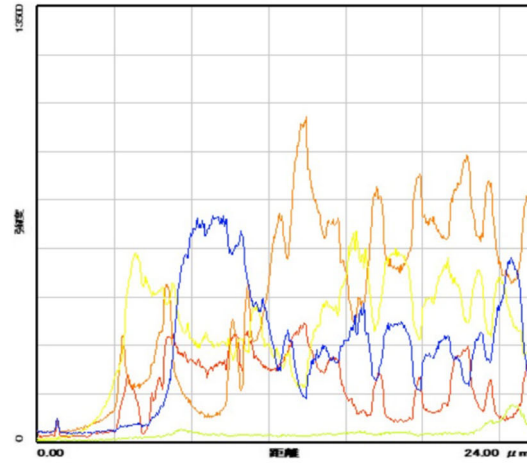
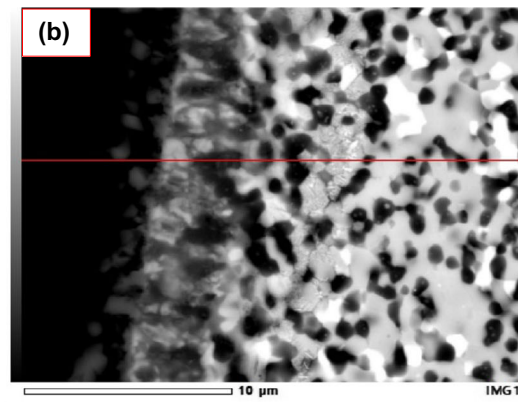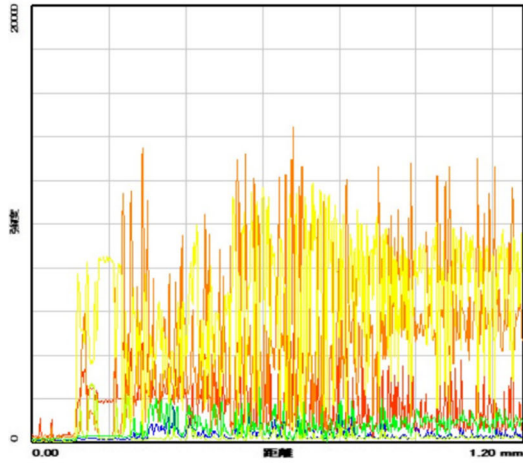$$2Al(s) + \frac{3}{2}O_2(g) \rightarrow Al_2O_3(s)$$

Ti diffusivity in TiO_2 is faster compared with oxygen, whereas Al has a slower diffusion rate in Al_2O_3 [35]. This leads to the outward growth of the rutile towards the gas-oxide interface while the Al_2O_3 grows inwards at the metal-oxide interface (or Al-rich side of the metal surface) [25]. This same process accounts for the formation of mixed TiO_2 and Al_2O_3 oxide films on the TiAl alloys subsurfaces [25] as evident in Fig. 7a–d and Fig. 8a and b.

Schmitz-Niederau and Schutze [36] reported that at temperatures higher than 973 K, TiO_2 cannot be considered as protective because of its porous structure and high growth rate while the development of a continuous Al_2O_3 barrier within the mixture of TiO_2 and Al_2O_3 offers controlled oxidation due to its dense nature and slow growth rate. TiO_2 is off-stoichiometric and often characterized with higher oxygen

Fig. 8 SEM SE and BSE images of oxides cross-section of **a, b** reference alloy; **c** alloy 1; **d** alloy 2; and **e, f** alloy 3 after isothermal oxidation testing 1273 K
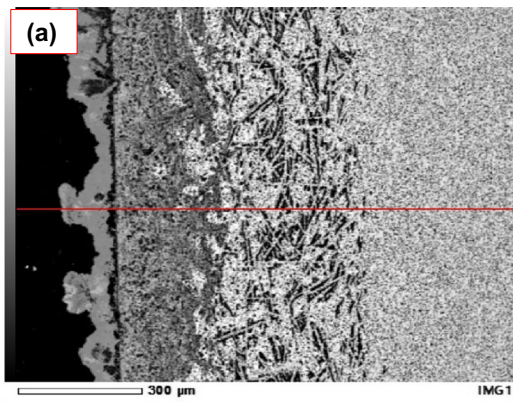
vacancies [37]. These oxygen vacancies typically serve as paths for fast diffusion of oxygen. This renders the formed rutile-structured TiO_2 oxide film unprotective and thus significantly limits the oxidation resistance of the reference alloy as observed from the mass change curves at 1123 K and 1273 K.

In the case of alloys 1, 2, and 3, the presence of 0.8, 4 and 8 at. % Ta tend to suppress the growth of the TiO_2 film. This stems from the hypothesis termed as the doping effect wherein the addition of a dopant element such as Ta with a valence electron (+5) higher than that of Ti (+4) decreases the defect concentration (or oxygen vacancy concentration) owing to the attainment of electroneutrality in the oxide [29, 38]. In other words, Ta addition retards the diffusion of oxygen in TiO_2, inhibiting internal oxidation.

This subsequently hinders the growth of the rutile and supports the establishment of a continuous and non-porous Al_2O_3 layer that acts as a diffusion barrier [39]. This probably explains the diminished XRD intensities of TiO_2 peaks, especially in alloys 2 and 3 compared with the reference alloy as seen in Fig. 4.

Furthermore, Song et al. [40] correlated the oxidation resistance of TiAl alloys to phase stability of the formed oxides and formation energy of oxygen vacancy. The authors asserted that the addition of elements with three d-electrons, such as Ta, increases the oxidation energy difference between Al_2O_3 and TiO_2 significantly. Hence, Ta addition tends to reduce the phase stability of Al_2O_3 relative to TiO_2 and increases the formation energy of oxygen vacancy [41]. The decreased phase stability of Al_2O_3 enhances oxidation resistance of TiAl alloys as observed in alloys 2 and 3 at both oxidation temperatures.

Nevertheless, the oxidation resistance of alloy 1 is quite like the reference alloy particularly at 1273 K. This may be ascribed to the low contents of Ta in the alloy, which probably does not adequately reduce oxygen solubility in alloy 1. Furthermore, at temperatures exceeding 1073 K when oxidized, Ta forms an intermediate reaction product of TaO resulting from a solid solution reaction with oxygen [42]. Usually, TaO forms at the metal-oxide interface [42]. As seen in Fig. 9c, alloy 1 forms mixed oxides of TaO and Al_2O_3 on the surface at 1273 K. TaO, however, tends to grow rapidly inwards and exhibits linear kinetics hence making the mixed oxides unprotective [43].

The findings in this study at 1123 K are in line with those of previous studies [44, 45].

Likewise, the impact of additions of 4 and 8 Ta (at. %) on enhancing the oxidation resistance in TiAl alloys at 1273 K has been investigated. Popela et al. [20] reported that at temperatures of 1273 K and higher, the presence of 8 at. % Ta in the studied Ti-46Al (at. %) alloy enhanced oxidation

resistance because of its ability to form a significantly denser, adherent and protective oxides. In parallel to a comparison study of Ti-44.8Al-6.6Ta and Ti-45.2Al-7.2Nb (at. %) alloys investigated by Vojtěch et al. [46], the efficacy of Ta to provide oxidation resistance in TiAl alloys at 1273 K was also attributed to the more stable and adherent oxides formed and the lower spallation tendency of these oxides.

The effects of Nb and Cr in inhibiting the formation and further growth of the TiO_2 in the reference alloy are not as pronounced as seen in the Ta containing alloys; however, the EDX analysis in Fig. 9 shows their presence in the reference alloy located underneath the Al_2O_3. It is well reported that the addition of Nb to TiAl alloys is mainly to improve oxidation resistance even as low as 2 at. % [47–50], and to some extent, the addition of Cr. Nb has a stronger β-stabilizing effect and enhances Al activity and diffusivity more efficiently compared with Ta. On the other hand, Ta has a slower diffusivity than Nb in TiAl alloys and hence reacts more slowly when exposed to oxidation [46] as noticed in Figs. 2 and 3. Additionally, from a thermodynamic stability perspective, the Gibbs free energy of formation of stable Ta_2O_5 and Nb_2O_5 oxides at 1473 K are -1413 kJ.mol^{-1} and -1256 kJ.mol^{-1}, respectively [51]. Ta_2O_5 has higher thermodynamic stability compared with $Nb_2O_{5.}$ Since Gibbs free energy of formation closely relates the strength of chemical bonds, Ta–O bonds may be deemed stronger than Nb–O bonds during oxidation and perhaps explains the variations in oxidation behaviors of the reference alloy and alloys 2 and 3. The inward diffusion of oxygen to the substrate may occur slowly in the Ta-containing alloys resulting in lower oxidation rates [46].

At temperatures exceeding 673 K, Cr forms Cr_2O_3 protective oxide with a corundum structure like Al_2O_3 [52]. Cr in TiAl alloys has been suggested to enhance the adhesion of oxide mixtures of Al_2O_3 and TiO_2 due to its solubility in Al_2O_3 and compatibility with TiO_2 [53]. Nonetheless, the best consideration of Cr incorporation is to enhance the plasticity of the reference alloy rather than its oxidation resistance, since their presence in low concentrations (< 4 at. %) has a detrimental effect on the oxidation resistance of TiAl intermetallics [54].

Figure 9 b and d show the presence of Ti in the Al_2O_3 formed on alloy 3. This is because Ti has quite a high solubility in Al_2O_3 [55]. Additionally, it effectively reduces the relative stability of Al_2O_3 over TiO_2, leading to the improvement of oxidation resistance of the alloy [55, 56].

5 Conclusion

The present study aims to evaluate the effect of Ta additions to the oxidation resistance of Ti-46.5Al (at. %) alloy. After oxidation tests at 1123 K and 1273 K, alloys with 4 and 8 at. % Ta

exhibit superior oxidation resistance compared with the 48-2-2 reference alloy and alloy with 0.8 at. % Ta.

The mass change of alloys 2 and 3 obey the parabolic growth law as their oxidation rate are nearly constant at both oxidation temperatures.

An evaluation of the cross-sections of the formed oxides made apparent that the formation of a non-porous outermost Al_2O_3 oxide culminates in the superior oxidation resistance behaviors of alloys with 4 and 8 at. % Ta. Furthermore, Ta additions of 4 and 8 at. % by doping effect suppress TiO_2 growth by decreasing oxygen vacancy concentrations and favors the establishment and growth of Al_2O_3. This protective oxide layer formed at the metal-oxide interface of the alloys, serve as a diffusion barrier which enhances the oxidation behaviors of the alloys at both tested temperatures.

Compliance with ethical standards

Conflict of interest The authors declare that they have no conflict of interest.

References

1. Appel F, Paul JDH, Oehring M (2011) Gamma titanium aluminide alloys: science and technology. Wiley
2. Clemens H, Mayer S (2013) Design, processing, microstructure, properties, and applications of advanced intermetallic TiAl alloys. Adv Eng Mater 15(4):191–215
3. Couret A, Molénat G, Galy J, Thomas M (2008) Microstructures and mechanical properties of TiAl alloys consolidated by spark plasma sintering. Intermetallics 16(9):1134–1141
4. Kothari K, Radhakrishnan R, Wereley NM (2012) Advances in gamma titanium aluminides and their manufacturing techniques. PrAeS 55:1–16
5. Jabbar H, Monchoux J-P, Houdellier F, Dollé M, Schimansky F-P, Pyczak F, Thomas M, Couret A (2010) Microstructure and mechanical properties of high niobium containing TiAl alloys elaborated by spark plasma sintering. Intermetallics 18(12):2312–2321
6. Jabbar H, Monchoux J-P, Thomas M, Couret A (2011) Microstructures and deformation mechanisms of a G4 TiAl alloy produced by spark plasma sintering. Acta Mater 59(20):7574–7585
7. Jabbar H, Monchoux J-P, Thomas M, Pyczak F, Couret A (2014) Improvement of the creep properties of TiAl alloys densified by spark plasma sintering. Intermetallics 46:1–3
8. Wu X (2006) Review of alloy and process development of TiAl alloys. Intermetallics 14(10–11):1114–1122
9. Kim D, Seo D, Huang X, Sawatzky T, Saari H, Hong J, Kim Y-W (2014) Oxidation behaviour of gamma titanium aluminides with or without protective coatings. Int Mater Rev 59(6):297–325
10. Hamzah E, Kanniah M, Harun M (2009) Effect of beta phase on room to high temperature mechanical properties of as-cast gamma titanium aluminide. Mech Adv Mater Struct 16(5):384–389
11. Huang Z, Cong T (2010) Microstructural instability and embrittlement behaviour of an Al-lean, high-Nb γ-TiAl-based alloy subjected to a long-term thermal exposure in air. Intermetallics 18(1):161–172
12. Liu Y, Li H, Wang S, Ye H (2009) Nb effects on the structural and mechanical properties of TiAl alloy: density-functional theory study. J Mater Res 24(10):3165–3173
13. Lu X, He X, Zhang B, Qu X, Zhang L, Guo Z, Tian J (2009) High-temperature oxidation behaviour of TiAl-based alloys fabricated by spark plasma sintering. J Alloys Compd 478(1–2):220–225
14. Mayer S, Erdely P, Fischer FD, Holec D, Kastenhuber M, Klein T, Clemens H (2017) Intermetallic β-solidifying γ-TiAl based alloys−from fundamental research to application. Adv Eng Mater 19(4):1600735
15. Braun R, Fröhlich M, Leyens C, Renusch D (2009) Oxidation behaviour of TBC systems on γ-TiAl based alloy Ti–45Al–8Nb. Oxid Met 71(5–6):295
16. Shida Y, Anada H (1993) The influence of ternary element addition on the oxidation behaviour of TiAl intermetallic compound in high temperature air. Corros Sci 35(5–8):945–953
17. McKee D, Huang S (1992) The oxidation behaviour of gamma-titanium aluminide alloys under thermal cycling conditions. Corros Sci 33(12):1899–1914
18. Okafor I, Reddy R (1999) The oxidation behaviour of high-temperature aluminides. JOM 51(6):35–40
19. Reddy RG, Li Y, Arenas MF (2002) Oxidation of a ternary Ti3Al-Ta alloy. High Temp Mater Process (London) 21(4):195–206
20. Popela T, Vojtěch D, Novák P, Knotek V, Průša F, Michalcová A, Novák M, Šerák J (2010) High-temperature oxidation of Ti-Al-Ta and Ti-Al-Nb alloys. Metal 18:1–4
21. Cobbinah PV, Matizamhuka WR (2018) The effect of SiC content on the corrosion and tribocorrosion performance of SPS produced Al-SiC nanocomposites. Afr Corros J 4:21–26
22. Laska N, Braun R, Knittel S (2018) Oxidation behavior of protective Ti-Al-Cr based coatings applied on the γ-TiAl alloys Ti-48-2-2 and TNM-B1. Surf Coat Technol 349:347–356
23. Bacos MP, Thomas M, Raviart JL, Morel A, Mercier S, Josso P (2011) Influence of an oxidation protective coating upon hot corrosion and mechanical behaviour of Ti–48Al–2Cr–2Nb alloy. Intermetallics 19(8):1120–1129
24. Fontana MG (2005) Corrosion engineering. Tata McGraw-Hill Education, New York
25. Kekare S, Aswath P (1997) Oxidation of TiAl based intermetallics. J Mater Sci 32(9):2485–2499
26. Mitoraj M, Godlewska E, Heintz O, Geoffroy N, Fontana S, Chevalier S (2011) Scale composition and oxidation mechanism of the Ti–46Al–8Nb alloy in air at 700 and 800 °C. Intermetallics 19(1):39–47
27. Haanappel VAC, Clemens H, Stroosnijder MF (2002) The high temperature oxidation behaviour of high and low alloyed TiAl-based intermetallics. Intermetallics 10(3):293–305
28. Rahmel A, Schütze M, Quadakkers W (1995) Fundamentals of TiAl oxidation–a critical review. Mater Corros 46(5):271–285
29. Pilone D, Felli F (2012) Isothermal oxidation behaviour of TiAl–Cr–Nb–B alloys produced by induction melting. Intermetallics 26:36–39
30. Kim BG, Kim GM, Kim CJ (1995) Oxidation behaviour of TiAl-X (X= Cr, V, Si, Mo or Nb) intermetallics at elevated temperature. ScMM 33(7):1117–1125
31. Zhao K, S-h O, Liu Y, Liu B, Liang X-p, H-z L, Wang Y (2019) Isothermal oxidation behavior of TiAl intermetallics with different oxygen contents. Trans Nonferrous Metals Soc China 29(3):526–533
32. Mathabathe MN, Bolokang AS, Govender G, Mostert RJ, Siyasiya CW (2018) The vacuum melted γ-TiAl (Nb, Cr, Si)-doped alloys and their cyclic oxidation properties. Vacuum 154:82–89
33. Dai J, Zhu J, Chen C, Weng F (2016) High temperature oxidation behaviour and research status of modifications on improving high temperature oxidation resistance of titanium alloys and titanium aluminides: a review. J Alloys Compd 685:784–798
34. Maurice V, Despert G, Zanna S, Josso P, Bacos MP, Marcus P (2007) XPS study of the initial stages of oxidation of α2-Ti3Al and γ-TiAl intermetallic alloys. Acta Mater 55(10):3315–3325

35. Pelachová T, Lapin J (2015) Cyclic oxidation behaviour of intermetallic Ti-46Al-8Ta alloy in air. Kovove Mater 53:415–422

36. Schmitz-Niederau M, Schutze M (1999) Cracking and healing of oxide scales on Ti-Al alloys at 900°C. Oxid Met 52(3):241–276

37. Kofstad P (1967) Note on the defect structure of rutile (TiO_2). J Less Common Metals 13(6):635–638

38. Taniguchi S, Shibata T (1996) Influence of additional elements on the oxidation behaviour of TiAl. Intermetallics 4:S85–S93

39. Lin J, Zhao L, Li G, Zhang L, Song X, Ye F, Chen G (2011) Effect of Nb on oxidation behaviour of high Nb containing TiAl alloys. Intermetallics 19(2):131–136

40. Song Y, Dai J, Yang R (2012) Mechanism of oxygen adsorption on surfaces of γ-TiAl. SurSc 606(9–10):852–857

41. Song Y, Xing F, Dai J, Yang R (2014) First-principles study of influence of Ti vacancy and Nb dopant on the bonding of $TiAl/TiO_2$ interface. Intermetallics 49:1–6

42. Kofstad P (1963) The oxidation behaviour of tantalum at 700–1000 C. JElS 110(6):491–501

43. Meier GH (1995) Research on oxidation and embrittlement of intermetallic compounds in the US. Weinheim, Oxidation of intermetallics. Wiley-VCH Verlag GmbH New York

44. Yuanyuan L, Weidong Z, Zhengping X, Xiaonan M, Yingli Y, Jinping W, Hangbiao S (2015) Microstructure, mechanical properties and oxidation behaviour of a hot-extruded TiAl containing Ta. Rare Metal Mater Eng 44(2):282–287

45. Popela T, Vojtěch D (2011) High-temperature behaviour of Ti-Al-Nb-Ta intermetallics. Metal 18:1–5

46. Vojtěch D, Popela T, Kubásek J, Maixner J, Novák P (2011) Comparison of Nb-and Ta-effectiveness for improvement of the cyclic oxidation resistance of TiAl-based intermetallics. Intermetallics 19(4):493–501

47. Haanappel V, Sunderkötter J, Stroosnijder M (1999) The isothermal and cyclic high temperature oxidation behaviour of Ti–48Al–2Mn–2Nb compared with Ti–48Al–2Cr–2Nb and Ti–48Al–2Cr. Intermetallics 7(5):529–541

48. Naveed M, Renteria AF, Weiß S (2017) Role of alloying elements during thermocyclic oxidation of β/γ-TiAl alloys at high temperatures. J Alloys Compd 691:489–497

49. Aniołek K, Kupka M, Łuczuk M, Barylski A (2015) Isothermal oxidation of Ti–6Al–7Nb alloy. Vacuum 114:114–118

50. Sihui O, Bin L, Jianbo L, Liyou X, Yong L (2015) Effect of Nb on high temperature oxidation behavior of powder metallurgy TiAl based alloy. Mater Sci Eng Powder Metallurgy 20(4):616–622

51. Gale W, Totemeier T, Gale W, Totemeier T (2004) Thermochemical data. Smithells Metals Reference Book, 8th edn. Elsevier Butterworth-Heinemann, Burlington, pp 24–26

52. Peter R, Saric I, Piltaver IK, Badovinac IJ, Petravic M (2017) Oxide formation on chromium metal surfaces by low-energy oxygen implantation at room temperature. TSF 636:225–231

53. He ZY, Wang ZX, Zhang F, Wang ZY, Liu XP (2013) Oxidation behavior of TiAl alloy treated by plasma surface chromizing process. Surf Coat Technol 228:S287–S291

54. Wang F, Tang Z, Wu W (1997) Effect of chromium on the oxidation resistance of TiAl intermetallics. Oxid Met 48(5–6):381–390

55. Ping F-P, Hu Q-M, Bakulin AV, Kulkova SE, Yang R (2016) Alloying effects on properties of Al_2O_3 and TiO_2 in connection with oxidation resistance of TiAl. Intermetallics 68:57–62

56. Becker S, Rahmel A, Schorr M, Schütze M (1992) Mechanism of isothermal oxidation of the intel-metallic TiAl and of TiAl alloys. Oxid Met 38(5–6):425–464